Electronics and Electrical Engineering

AIMS Electronics and Electrical Engineering, 10(3): 527–542
DOI: 10.3934/electreng.2026021
Received: 24 January 2026
Revised: 20 March 2026
Accepted: 03 June 2026
Published: 02 July 2026

https://www.aimspress.com/journal/ElectrEng

Research article

Trajectory tracking control for three-wheeled mobile robots (TWMR) considering wheel slip effect

Long Q. Dinh[1], Dung T. Nguyen[1], Duc M. Ngo[2], Mui D. Nguyen[2], Hung T. Nguyen[2], Ha T. Nguyen[1], Thang C. Vu[1] and Minh T. Nguyen[2,*]

[1] Thai Nguyen University of Information and Communications Technology, Thai Nguyen, Viet Nam
[2] Thai Nguyen University of Technology, Thai Nguyen University, Thai Nguyen, Viet Nam

*** Correspondence:** Email: nguyentuanminh@tnut.edu.vn.

Abstract: The development of robot technology has received increased interest in three-wheeled mobile robots (TWMR) due to their flexibility and adaptability in various applications. However, due to the limitation of independent motion in all directions, highly nonlinear dynamics, and effects such as noise and wheel slippage, it is difficult to effectively control the motion of TWMR. In this paper, we studied the motion of TWMR through kinematic and dynamic models considering the phenomenon of wheel slippage. The lateral and longitudinal slippage components were added to the dynamic model, thereby designing the position control law using the backstepping method and the speed control law using the SMC method. We also adjusted the parameters of the controllers to help the robot perform trajectory tracking. In addition, controlling the input torque was performed to overcome the lateral and longitudinal slippage phenomena. The method was tested through simulations on MATLAB Simulink with different trajectory cases (circular trajectory, infinite trajectory, spiral trajectory). The results showed the suitability of the controller to the desired trajectory tracking problem of TWMR, and the trajectory tracking error converged to zero. This shows promise and is practical.

Keywords: TWMR; backstepping; sliding mode control (SMC); follow the set trajectory; wheel slippage

1. Introduction

The development of robotics technology has received increased interest in three-wheeled

mobile robots (TWMRs) due to their versatility and adaptability across a wide range of applications. However, effectively controlling TWMRs remains a significant challenge due to their inherent non-universal limitations; the ability to move independently in all directions. Environmental factors affecting robot operation such as sensor interference, nonlinear dynamic systems, and variations in system parameters add to the complexity of TWMR motion control [1–3].

The field of trajectory tracking control of wheeled mobile robots has been the focus of extensive research efforts [4–6]. Achieving efficient position estimation techniques is essential for mobile robots to navigate effectively, especially in environments where sensor measurements are noisy. Localization is also an important aspect of mobile robots, enabling robots to extract information from sensors, determine their position, plan actions, and control movement effectively [7–9].

With advancements in control algorithms, including Proportional-Integral-Derivative (PID) control, Sliding Mode Control (SMC), and Model Prediction Control (MPC), TWMR has achieved higher autonomy [10–12]. Two-wheel differential-driven mobile robots (DDMR) were used in [13] to track trajectories in various scenarios. The trajectory tracking controller is presented in [14], which was used to reliably instruct a wheeled mobile robot (WMR) to follow a predetermined path for a finite period of time when disturbances were present. Kinematic equations were used to model the two-wheeled mobile robot and track the error. System models were then used to test the stability and accessibility of the sliding mode controller. In [15], the SMC application was used to determine the optimal control strategy for operating time, trajectory error, and energy consumption for the MWOMR mobile robot. The researchers in [16] proposed a backstepping-based kinematic-torque combined control framework for non-orthogonal robots, ensuring asymptotic stability according to Lyapunov. Furthermore, an adaptive controller based on neural networks was used to handle disturbances and unknown dynamics.

When developing kinematic and dynamic models of TWMRs, pure rolling (no slippage) is often considered the limiting constraint. However, when TWMRs move at high speeds or on surfaces with low friction, slippage is unavoidable. To date, many studies have been conducted on TWMRs with and without considering wheel slippage. In [17], the authors used a traction model in which the coefficient of adhesion between the wheels and the hard flat surface was a function of slip. Simulations of the controller study that did not account for slip had poorer performance and larger deviations. The authors in [18] proposed a new method to track the path of the WMR when there is an unknown lateral slip. Reinforcement learning (RL) and position-based direction estimation (LTE) were used to calculate the possible position of the WMR. In addition, a DecaWave-based distance measurement system was also used to update the weights for the particle filter PF. The information about the desired trajectory was used to develop an algorithm to extract the lateral slip along the x and y axes.

The major contributions of this work are provided as follows:

• We study the kinematic and dynamic models of TWMR with and without slippage, determining traction based on wheel dynamics.

• We develop a control law to track the desired trajectory based on a combination of backstepping and SMC for the position and speed of the TWMR. We control the motor torque to overcome wheel slippage.

• We build MATLAB and Simulink models to verify the results with different scenarios.

The rest of this work is organized as follows: The kinematic and dynamic models considering the sliding effect are provided in Section 2. The design of the controllers is addressed in Section 3. Some simulation results with analysis are provided in Section 4. Discussion about the results and

comparison with other work are provided in Section 5. Finally, conclusions and future work are addressed in Section 6.

2. TWMR kinematics and dynamics model considering sliding effects

2.1. Kinematics

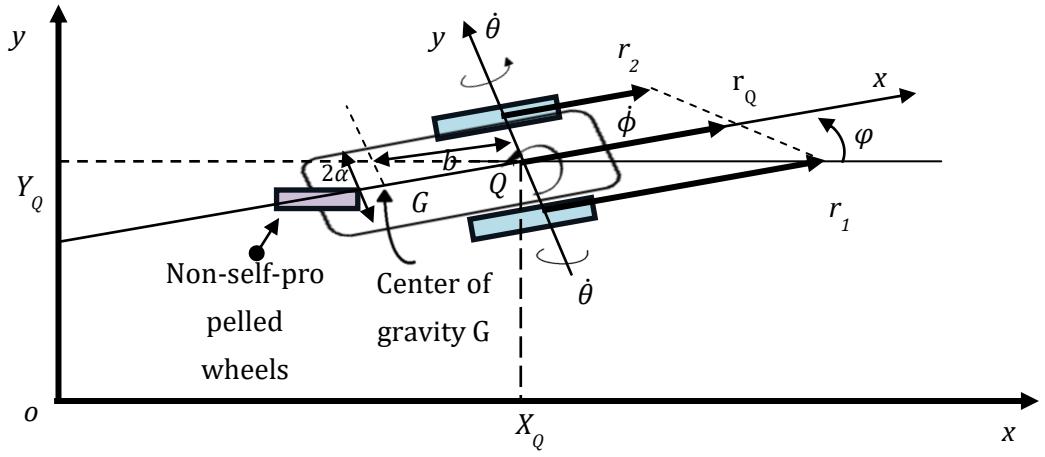

Figure 1. TWMR mobile robot.

The geometry and kinematic parameters of the TWMR are shown in Figure 1. The WMR's position vector (position/orientation) and its velocity are, respectively:

$$\mathrm{q} = \begin{bmatrix} x_Q \\ y_Q \\ \phi \end{bmatrix}, \dot{\mathrm{q}} = \begin{bmatrix} \dot{x}_Q \\ \dot{y}_Q \\ \dot{\phi} \end{bmatrix} \tag{1}$$

Let v_1 and v_r be the linear velocities of the left and right wheels, respectively, and let v be the velocity of the midpoint of the wheel v_Q of the TWMR. Then, from Figure 1, we have:

$$v_{\mathrm{r}} = v_Q + a\dot{\theta}, v_{\mathrm{l}} = v_Q - a\dot{\theta} \tag{2}$$

Adding and subtracting v_r and v_1 gives

$$v_Q = 0.5(v_{\mathrm{r}} + v_{\mathrm{l}}), \qquad 2a\dot{\theta} = 2a\omega = v_{\mathrm{r}} - v_{\mathrm{l}} \tag{3}$$

We have $v_{\mathrm{r}} = r\dot{\theta}_{\mathrm{r}}$ and $v_{\mathrm{l}} = r\dot{\theta}_{\mathrm{l}}$. r is the radius of the robot's wheel which is defined as r = 0.1 m.

The kinematic model can be obtained by expressing the TWMR velocity in terms of the linear and angular velocities of the TWMR in the robot frame as follows:

$$\dot{\mathrm{p}} = \begin{bmatrix} \dot{x}_Q \\ \dot{y}_Q \\ \dot{\theta} \end{bmatrix} = \begin{bmatrix} \cos(\theta) & 0 \\ \sin(\theta) & 0 \\ 0 & 1 \end{bmatrix} \begin{bmatrix} v \\ w \end{bmatrix} \tag{4}$$

Non-uniform constraints $-\dot{x}_Q sin\phi + \dot{y}_Q cos\phi = 0$ (5)

2.2. Dynamics

The dynamic model of WMR is described as follows:

$$\frac{d}{dt}\left(\frac{\partial L}{\partial \dot{q}_k}\right) - \frac{\partial L}{\partial q_k} + \frac{\partial P}{\partial \dot{q}_k} + g_k + \tau_{d_k} = f_k \tag{6}$$

where the index k describes the general coordinate q_k $(k = 1, \ldots, n), L$ determines the Lagrange (difference between the kinetic and potential energy of the system), P is the power dissipation function due to friction and damping in the system, g_k is the gravitational force, τ_{d_k} is the system disturbance, and f_k is the resultant force (external influence on the system) related to the general coordinate q_k. (6) is valid only for an unconstrained system with no degrees of freedom and no velocity constraints.

For systems with motion constraints, the dynamic equations are derived using the Lagrange multiplier as follows:

$$\mathrm{M(q)\ddot{q} + V(q,\dot{q})\dot{q} + F(\dot{q}) + G(q) + \tau_d = B(q)\tau - \Lambda^T(q)^{\lambda}} \tag{7}$$

In this case, $M(q)$ is the $n \times n$ symmetric positive definite inertia matrix, $V(q, \dot{q})$ is the centripetal and Coriolis matrix, $G(q)$ is the gravitational force vector, τ_d is the bounded perturbation vector, $B(q)$ is the input matrix, τ is the input vector, $\Lambda^T(q)$ is the matrix associated with the kinematic constraints, and λ is the Lagrange multiplication vector. For TWMR, the general coordinates are chosen as:

$$\dot{q} = [\dot{x} \quad \dot{y} \quad \dot{\theta}]^T \tag{8}$$

The parameter matrices and vectors are given as follows:

$$\mathrm{M(q)} = \begin{bmatrix} \mathrm{m} & 0 & 0 \\ 0 & \mathrm{m} & 0 \\ 0 & 0 & \mathrm{I} \end{bmatrix} \tag{9}$$

$$\Lambda^T(q) = \begin{bmatrix} m & 0 & 0 \\ 0 & m & 0 \\ 0 & 0 & I \end{bmatrix} \begin{bmatrix} -\sin(\theta) \\ \cos(\theta) \\ 0 \end{bmatrix} = \begin{bmatrix} -\mathrm{m}\sin(\theta) \\ m\cos(\theta) \\ 0 \end{bmatrix} \tag{10}$$

$$B(q) = \frac{1}{r}\begin{bmatrix} \cos(\theta) & \cos(\theta) \\ \sin(\theta) & \sin(\theta) \\ 2a & -2a \end{bmatrix} \tag{11}$$

$$\tau = \begin{bmatrix} \tau_r \\ \tau_l \end{bmatrix}, \tag{12}$$

where m is the mass of the TWMR, and I is the moment of inertia of the TWMR around its center. τ_R and τ_L are the torques of the right and left DC motors, respectively.

The main objective is to eliminate the constraint $\Lambda^T(q)\lambda$ in equation (1.27) since the Lagrange multipliers λ_i are unknown. Using the matrix $S(q)$ of $n \times (n - m)$, we get:

$$S^T(q)\Lambda^T(\mathrm{q}) = 0 \ \text{vậy} \ S(q) = \begin{bmatrix} \cos\theta & 0 \\ \sin\theta & 0 \\ 0 & 1 \end{bmatrix} \tag{13}$$

From the non-total constraint $\Lambda\dot{\mathrm{p}} = 0 \, với \, \Lambda = [-sin\theta \quad cos\theta \quad 0]$, it can be seen that there exists a vector η (t)= $[\dot{\phi}_r \quad \dot{\phi}_l]^T$ with direction (n × m) such that: $\dot{\mathrm{p}}(t) = S(q)\eta(t)$. Next, taking the time derivative, we have: $\ddot{q} = \dot{S}(q)\eta + S(q)\dot{\eta}$. Substituting into (7), we have

$$M(q)\left[\dot{S}(q)\eta + S(q)\dot{\eta}\right] + V(q,\dot{q})[S(q)\eta] + F(\dot{q})[S(q)\eta] = B(q)\tau - \Lambda^T(q)\lambda \tag{14}$$

Multiplying both sides by $S^T(q)$ gives:

$$S^T(q)M(q)S(q)\dot{\eta} + S^T(q)\left[M(q)\dot{S}(q) + V(q,\dot{q})S(q)\right]\eta + F(\dot{q})[S(q)\eta] = S^T(q)B(q)\tau - S^T(q)\Lambda^T(q)\lambda \tag{15}$$

$$\hat{M}(q)\dot{\eta} + \hat{V}(q,\dot{q})\eta + \hat{F}(\dot{q}) = \hat{B}(q)(\tau + \hat{\tau}_d) \tag{16}$$

where $\hat{M} = S^T M S$, $\hat{F} = S^T F$, $\hat{B} = S^T B$, and $\hat{\tau}_d = S^T \tau_d$ is the external disturbance. Assuming the distance between the centroid and the coordinate center of TWMR is 0, this leads to $\hat{V}(q,\dot{q}) = 0$. Additionally, considering the surface friction $F(\dot{q})$ and the external disturbance (τ_d) are also equal to 0, Equation (16) becomes:

$$\begin{bmatrix} m & 0 \\ 0 & \mathrm{I} \end{bmatrix}\begin{bmatrix} \dot{v} \\ \dot{w} \end{bmatrix} = \frac{1}{r}\begin{bmatrix} 1 & 1 \\ 2a & -2a \end{bmatrix}\begin{bmatrix} \tau_{\mathrm{r}} \\ \tau_l \end{bmatrix} \tag{17}$$

Now, if we consider the wheel slippage phenomena and incorporate the robot's wheel model into the dynamic model, assuming the center of gravity is the position point, then the equations of motion can be written in the following form:

$$\mathrm{M}(q)\ddot{q} + \mathrm{V}(q,\dot{q})\dot{q} = \mathrm{B}(q)\tau + \Lambda^T(q)\lambda \tag{18}$$

$$\mathrm{M}(q) = \begin{bmatrix} m_t & 0 & -ma\sin\theta & 0 & 0 \\ 0 & m_t & ma\cos\beta\theta & 0 & 0 \\ -ma\sin\theta & ma\cos\theta & I_t & 0 & 0 \\ 0 & 0 & 0 & I_w & 0 \\ 0 & 0 & 0 & 0 & I_w \end{bmatrix},$$

$$\mathrm{V}(q,\dot{q}) = \begin{bmatrix} 0 & 0 & -ma\,\dot{\theta}\cos\theta & 0 & 0 \\ 0 & 0 & -ma\,\dot{\theta}\sin\theta & 0 & 0 \\ 0 & 0 & 0 & 0 & 0 \\ 0 & 0 & 0 & 0 & 0 \\ 0 & 0 & 0 & 0 & 0 \end{bmatrix}, \mathrm{B}(q) = \begin{bmatrix} 0 & 0 \\ 0 & 0 \\ 0 & 0 \\ 1 & 0 \\ 0 & 1 \end{bmatrix},$$

$$\Lambda^T(q)\lambda = \begin{bmatrix} -\sin\theta & \cos\theta & \cos\theta \\ \cos\theta & \sin\theta & \sin\beta \\ 0 & a & -a \\ 0 & -R & 0 \\ 0 & 0 & -R \end{bmatrix} \times \begin{bmatrix} \lambda_1 \\ \lambda_2 \\ \lambda_3 \\ \lambda_4 \\ \lambda_5 \end{bmatrix}$$

where I_w represents the moment of inertia of the robot wheel with respect to its axis of rotation, and λ_i are the lag factors.

3. Controller design

Our goal is to develop a controller to improve the accuracy of trajectory tracking for TWMR. The idea is to utilize the outstanding advantages of backstepping and SMC controllers to address the

difficulties of the TWMR model, such as the nonlinearity of dynamics, the limitations of non-uniformity, and the influence of wheel slip. The SMC is designed as the controller for the dynamic element of the TWMR, while the backstepping controller is used for the dynamic element of the TWMR to perform trajectory tracking.

3.1. Backstepping controller

Consider the reference trajectory as a function that satisfies the robot's continuity and differentiability condition.

We have:
$$x = x_r(t), y = y_r(t), \theta = \theta_r(t) \tag{19}$$

Taking the derivative, we have:

$$\dot{x}_r(t) = v_r(t)\cos\big(\theta_r(t)\big), \dot{y}_r(t) = v_r(t)\sin\big(\theta_r(t)\big),\ \dot{\theta}_r(t) = \omega_r(t) \tag{20}$$

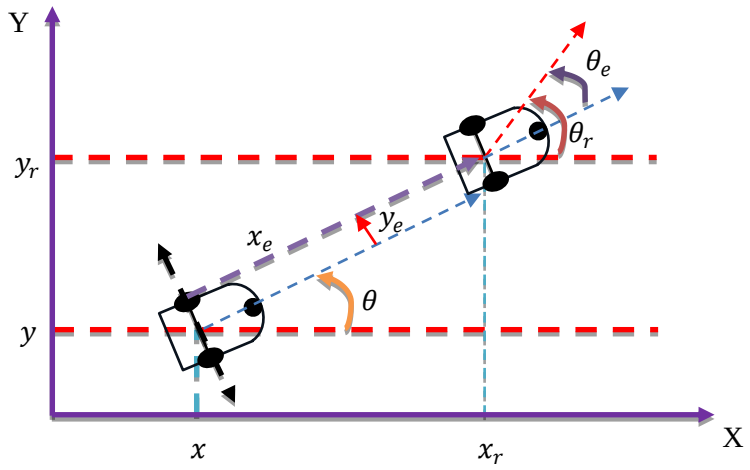

Figure 2. Position error of TWMR relative to the reference trajectory.

The trajectory tracking error is shown in Figure 2, as can be seen:

$$p = \begin{bmatrix} x_e \\ y_e \\ \theta_e \end{bmatrix} = \begin{bmatrix} \cos(\theta) & \sin(\theta) & 0 \\ -\sin(\theta) & \cos(\theta) & 0 \\ 0 & 0 & 1 \end{bmatrix} \begin{bmatrix} x_r - x \\ y_r - y \\ \theta_r - \theta \end{bmatrix}, \tag{21}$$

$$\begin{aligned} x_e &= \cos(\theta)\,(x_r - x) + \sin(\theta)(y_r - y), \\ y_e &= -sin(\theta)\,(x_r - x) + cos(\theta)(y_r - y), \\ \theta_e &= \theta_r - \theta. \end{aligned} \tag{22}$$

Taking the derivative of Eq (20) and substituting it back in, we get the trajectory tracking error as:

$$\begin{aligned} \dot{x}_e &= \dot{\theta} y_e + v_r\, cos(\theta_e) - v = \omega y_e + v_r\, cos(\theta_e) - v \\ \dot{y}_e &= -\dot{\theta} x_e + v_r\, sin(\theta_e) = -\,\omega x_e + v_r\, sin(\theta_e) \\ \dot{\theta}_e &= \dot{\theta}_r - \dot{\theta} = \omega_r - \omega \end{aligned}$$

$$\begin{bmatrix}\dot{x}_e\\ \dot{y}_e\\ \dot{\theta}_e\end{bmatrix}=\begin{bmatrix}\omega y_e+v_r\,cos(\theta_e)-v\\ -\omega x_e+v_r\,sin(\theta_e)\\ \omega_r-\omega\end{bmatrix} \tag{23}$$

where v and ω are the desired linear and angular velocities at the output of the Backstepping Controller.

Select the Lyapunov function as follows:

$$V=\frac{1}{2}(x_e^2+y_e^2)+\frac{1-\cos(\theta_e)}{k_2} \tag{24}$$

$$\dot{V}=x_e\dot{x}_e+y_e\dot{y}_e+\frac{\dot{\theta}_e\sin(\theta_e)}{k_2} \tag{25}$$

$\dot{V}=(u_2y_e+v_r\cos(\theta_e)-u_1)x_e+(-\dot{\theta}x_ev_r\sin(\theta_e)\,y_e+\frac{(\dot{\theta}_r-u_2)\sin(\theta_e)}{k_2}$, select the control signal $(u=[u_1u_2]^T=(v,\omega)^T$ such that the derivative of the candidate Lyapunov function is less than or equal to zero ($\dot{V}\le 0$).

$$\begin{aligned}u_1&=v_r\cos(\theta_e)+k_1x_e\\ u_2&=\dot{\theta}_r+v_r(k_2y_e+k_3\sin(\theta_e))\end{aligned} \tag{26}$$

Backstepping controller for the kinematic model of the outer ring:

$$\begin{bmatrix}v\\ \omega\end{bmatrix}=\begin{bmatrix}u_1\\ u_2\end{bmatrix}=\begin{bmatrix}v_r\cos(\theta_e)+k_1x_e\\ \omega_r+v_r(k_2y_e+k_3\sin(\theta_e))\end{bmatrix} \tag{27}$$

The parameters (k_1, k_2, k_3) > 0 are conditions for controller stability; they directly affect the convergence rate and overcorrection of the error.

3.2. SMC controller design

With its good noise response capabilities [19,20], the SMC method is chosen to enable zero tracking error of the dynamic controller. The velocity error is given as follows:

$$E_v=v_d-v,\ E_\omega=\omega_d-\omega \tag{28a, b}$$

Taking the derivative, we have:

$$\dot{E}_v=\dot{v}_d-\dot{v}=\dot{v}_d-\frac{F_1}{\mathrm{m}},\ \dot{E}_\omega=\dot{\omega}_d-\dot{\omega}=\dot{\omega}_d-\frac{\tau_2}{\mathrm{I}} \tag{29a, b}$$

Choose the input force and torque as follows: $F_1=\mathrm{m}\dot{v}_d+k_aE_v,\ \tau_2=\mathrm{I}\dot{\omega}_d+k_bE_\omega$. The velocity error equation will be $\mathrm{m}\dot{E}_v+k_aE_v=0,\ \mathrm{I}\dot{E}_\omega+k_bE_\omega=0$. If the coefficients k_a and k_b > 0, then the inertial velocity error and angular velocity error (E_v,E_ω) stabilize and converge to 0. Then we have the moment of the two wheels as:

$$\tau_R=\left(F_1-\frac{1}{2a}\tau_2\right)\frac{R}{2},\ \tau_L=\left(F_1+\frac{1}{2a}\tau_2\right)\frac{R}{2} \tag{30}$$

3.3. Torque control to prevent slippage

By assuming a hard ground and a hard wheel, the wheel equation is $m_w\,a_w=F_{long}$, where F_{long} is the axial force. The linear acceleration during pure rolling is $a_w=\mathrm{R}\,\ddot{\gamma}$. For each wheel, we have $I_{wy}\,\ddot{\gamma}=\tau-R\,F_{long}$.

From this, we have:

$$F_{long} = \frac{\tau\, m_w\, \mathrm{R}}{m_w\, \mathrm{R}^2 + I_{wy}} \tag{31}$$

If $F_{long} > F_{long}^{s}$, slippage occurs, so the axial force needs to be limited to static friction as follows:

$$\mu_s \mathrm{N} = \frac{\tau\, m_w\, R}{m_w\, R^2 + 2\, I_{wy}} \tag{32}$$

Due to the unevenness in the contact area between the wheel and the ground, we consider Coulomb's friction model [21,22]. This unevenness acts as anchors that need to be broken by maximum force to produce relative motion between the wheel and the ground. Therefore, we use the static friction coefficient (μ_s) with the normal reaction force on the wheel to estimate the value of the force needed to be applied to the wheel before sliding $\left(F_{long}^{s}\right) = \mu_s \mathrm{N}$. From this, we can calculate the maximum torque, and the torque of the left and right wheels is limited by:

$$\tau_{max} = \frac{\mu_s\, \mathrm{N}\left(m_w\, R^2 + 2\, I_{wy}\right)}{m_w\, R} \tag{33}$$

$$\tau_{maxR} = \frac{\mu_s\, \mathrm{N}_R\left(m_w\, R^2 + 2\, I_{wy}\right)}{m_w\, R} \tag{34}$$

$$\tau_{maxL} = \frac{\mu_s\, \mathrm{N}_L\left(m_w\, R^2 + 2\, I_{wy}\right)}{m_w\, R} \tag{35}$$

If $\tau_R, \tau_L < \tau_{maxR}, \tau_{maxL}$, the controller applies torque. If $\tau_R, \tau_L < \tau_{maxR}, \tau_{maxL}$ the control inputs are applied in the form of torques. If $\tau_R, \tau_L > \tau_{maxR}, \tau_{maxL}$, then τ_R, τ_L is limited to the maximum torque value.

The trajectory tracking process is shown in the block diagram in Figure 3, with the simulation variables calculated as above.

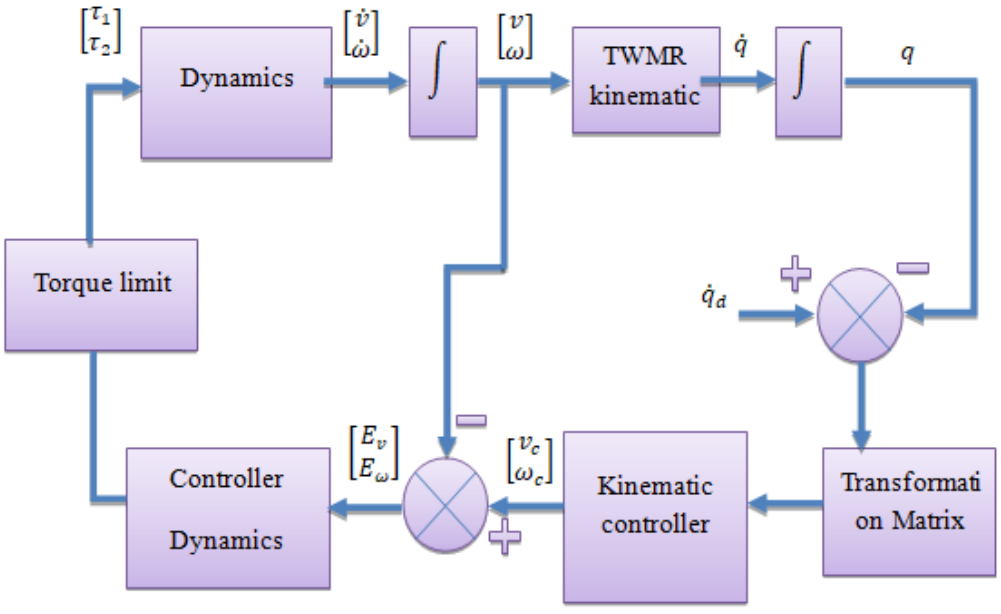

Figure 3. Diagram of the robot trajectory tracking process.

The simulation diagram of the trajectory tracking controller in Simulink is shown in detail in Figure 4.

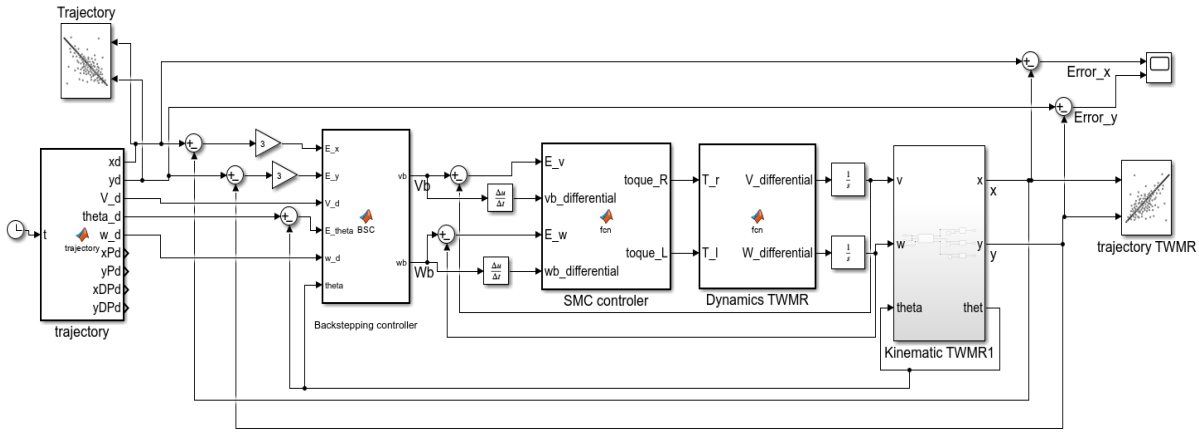

Figure 4. Simulink simulation diagram.

4. Simulation results

Table 1. Robot parameters and constants.

	Symbol	Unit	Value
Wheel radius	R	m	0.0635
Robot weight	m	kg	10
Wheel weight	m_r	m	1
Static friction coefficient	μ	-	0.7
Normal force acting on the wheel	N_r	N	98.1
Robot wheelbase	a	m	0.1

The circular reference orbit has a radius of 10 m, with the center at coordinates (0,0). The mathematical representation is xd = 10*cos(ω*t), yd = 10*sin(ω*t). The TWMR's trajectory along the set orbit is shown in Figure 5 (b). Position deviations are shown in Figures 6 and 7.

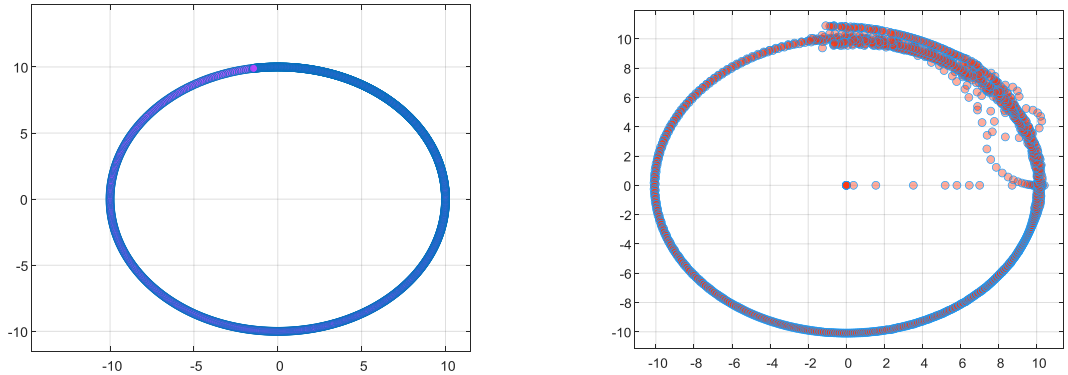

(a) (b)

Figure 5. Circular reference trajectory (a) and TWMR travel trajectory (b).

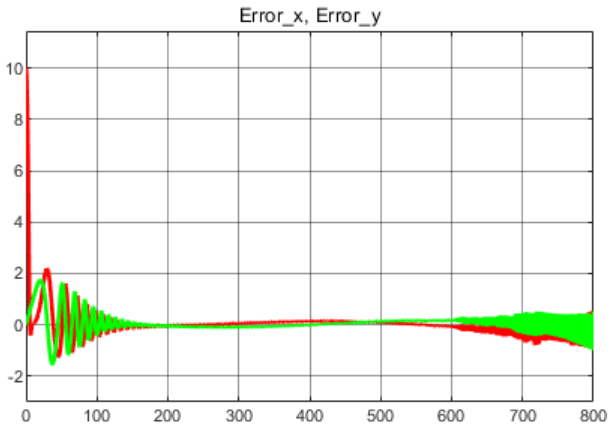

Figure 6. Circular tracking error of TWMR.

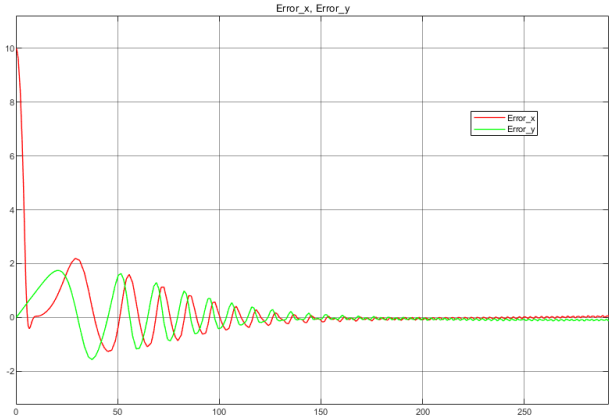

Figure 7. Details of the convergence times of the x and y deviations along the circular trajectory.

The x-axis and y-axis deviations of the SMC controller are compared with the FOPID controller, as shown in Figure 8.

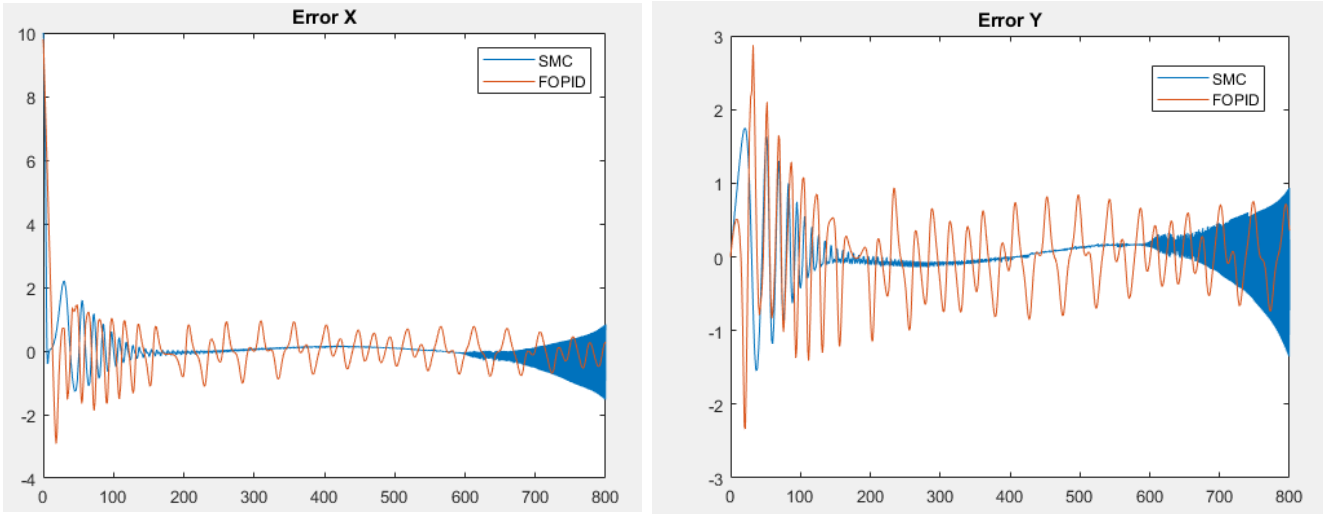

(a) (b)

Figure 8. Comparison of the positional deviations along the x (a) and y (b) axes with the circular trajectory.

Simulation results show that with a relatively large orbital radius, the controller helps the TWMR track the set trajectory with zero convergence position error. Although the robot starts at the center of the orbit, far from the starting point, the speed and convergence time are still acceptable.

The spiral trajectory has the following form:

$$xd = (1.5+0.05*t)*\cos(\omega*t); \quad (36)$$

$$yd = (1.5+0.05*t)*\sin(\omega*t); \quad (37)$$

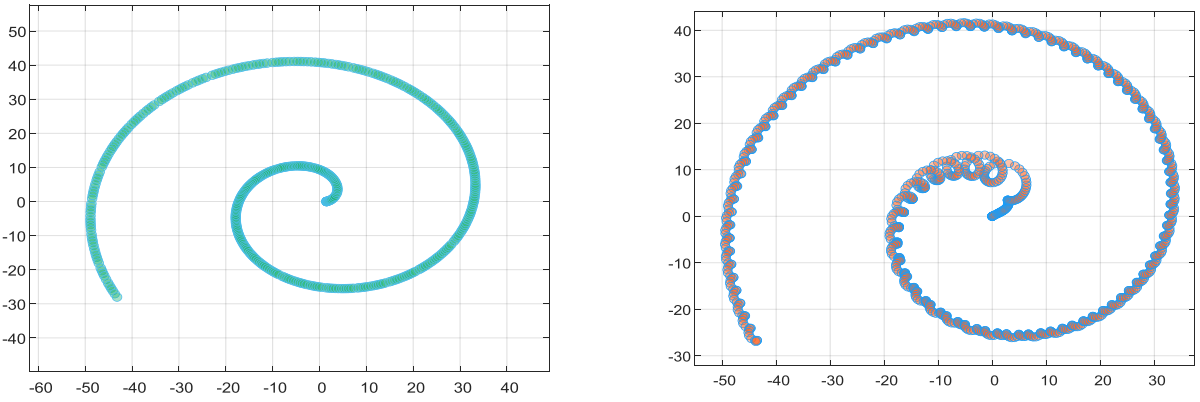

(a) (b)

Figure 9. Reference helical trajectory (a) and TWMR output response to reference trajectory (b).

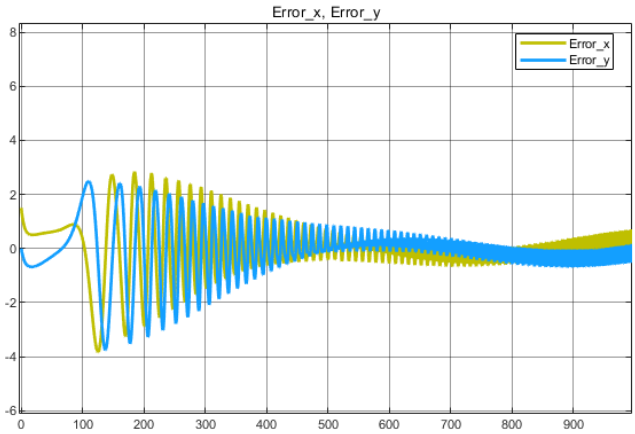

Figure 10. Position deviation of the TWMR spiral trajectory.

The x-axis and y-axis deviations of the SMC controller compared to the FOPID controller in the helical trajectory are shown in Figure 11.

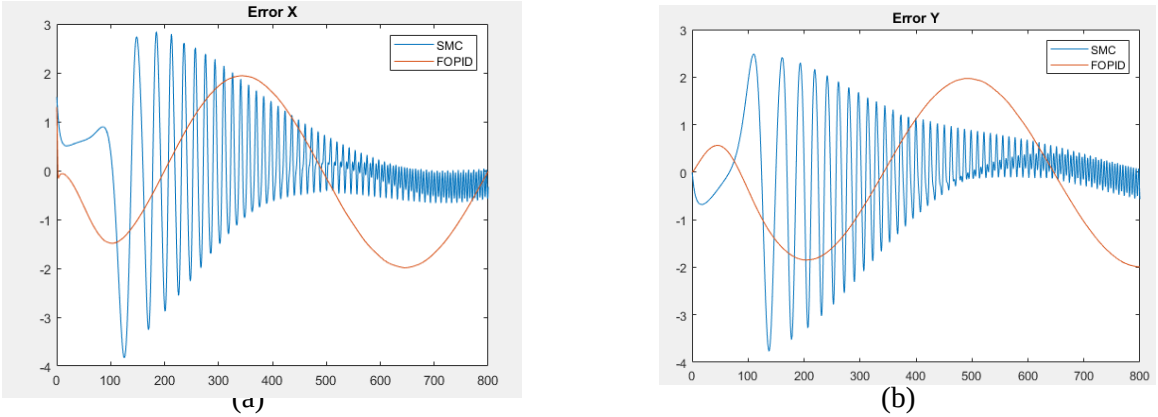

(a) (b)

Figure 11. Comparison of x-axis (a) and y-axis (b) position errors of SMC and FOPID controllers in a helical trajectory.

The helical trajectory also demonstrates the effectiveness of the designed controller. Due to the

characteristic of the helical trajectory, where the angular acceleration changes continuously over time, the smoothness of the tracking trajectory is not as expected. However, the positional error of the trajectory has converged to zero, as designed.

The infinite trajectory has the form: xd = 1+10*cos((2*3.14/105) *t); yd = 5*sin((4*3.14/105) *t). The robot has the corresponding initial position (x, y, θ) = (1, 0, pi/4). The reference trajectory is shown in Figure 12 (a), and the response trajectory of the TWMR is shown as in Figure 12 (b).

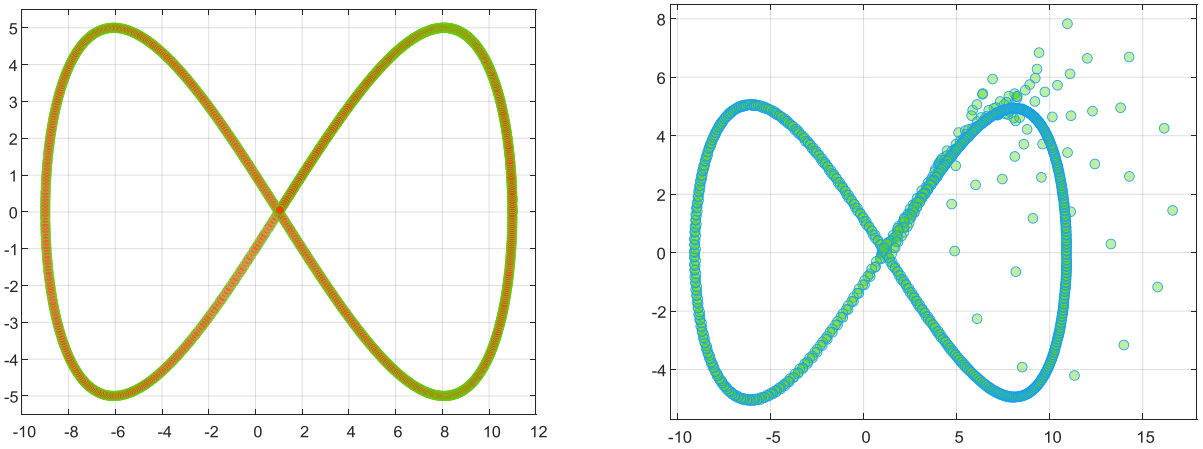

(a) (b)

Figure 12. Infinite-form reference orbit (a) and TWMR orbital response (b).

The tracking error of the controller is shown in Figure 13. The difference between the desired velocity and the actual velocity is expressed as E_v and E_w. Details are shown in Figure 14.

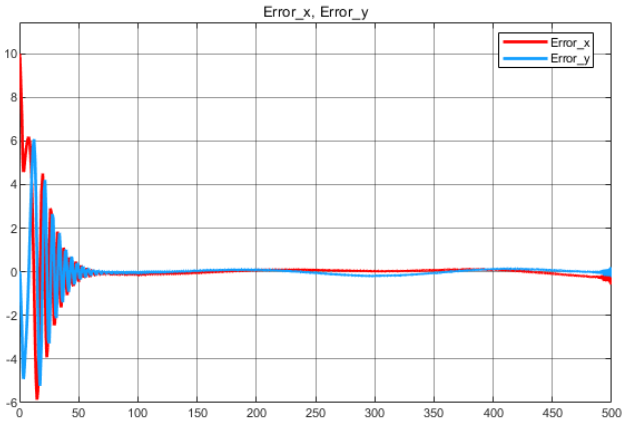

Figure 13. Position deviation of TWMR at infinity orbit.

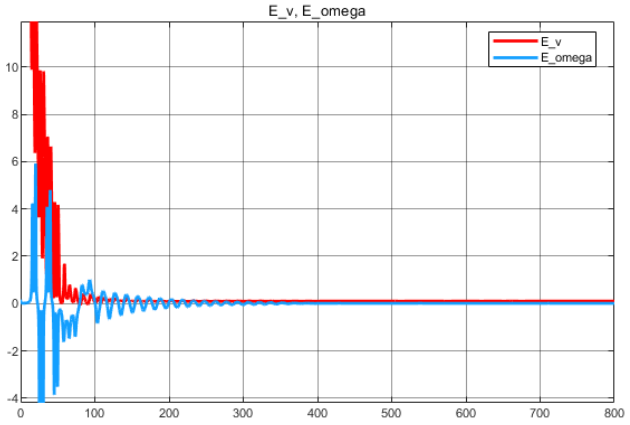

Figure 14. Angular velocity and linear velocity deviations of SMC.

The x-axis and y-axis deviations of the SMC controller compared to the FOPID controller in infinite orbit are shown in Figure 15.

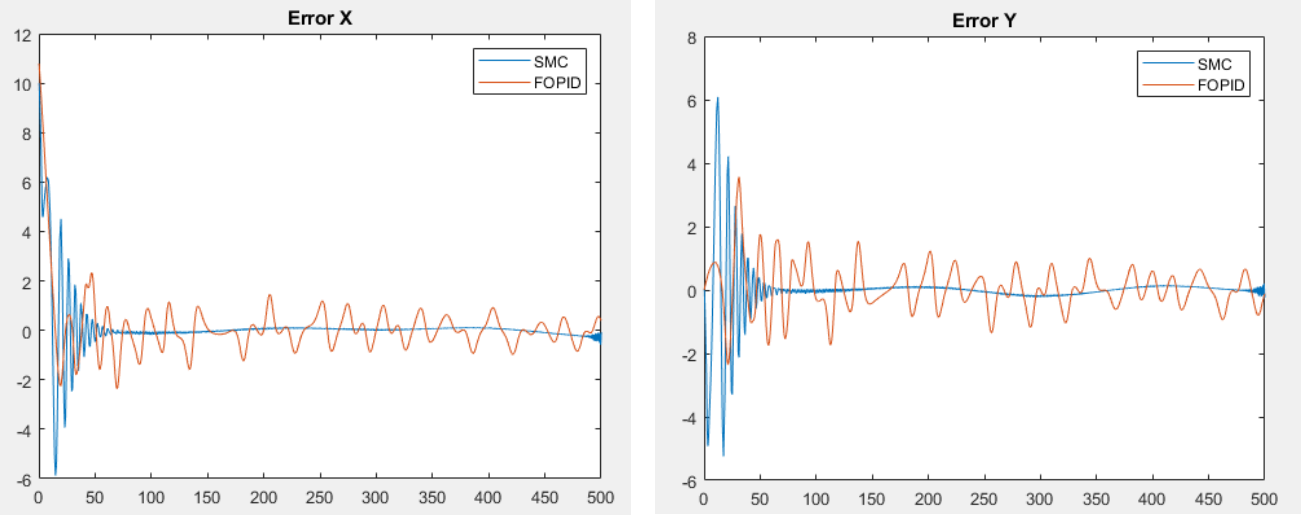

(a) (b)

Figure 15. Comparison of x-axis (a) and y-axis (b) position errors of SMC and FOPID controllers in infinite orbit.

The RMSE index is used to evaluate the performance of the SMC controller compared to FOPID in different orbits. Details are presented in Table 2.

Table 2. Summary and comparison of the RMSE index with different trajectories.

	Circle	**Spiral**	**Infinity**
RMSE_SMC	0.866628	1.380615	1.422575
RMSE_FOPID	0.987921	1.893160	1.657791

Simulation results show that SMC consistently has a smaller RMSE than FOPID on all three orbits, demonstrating better tracking capability. The error increases with more complex orbits (spirals, infinity), especially with FOPID. However, the RMSE is still relatively accurate, so further adjustments are needed to improve accuracy.

5. Discussion

One of the significant contributions of this research is the construction and simulation of a hierarchical controller for a TWMR, in which a backstepping controller is used for the position link and a sliding mode controller (SMC) is applied to the velocity link, based on a dynamic model that considers the wheel slip effect. The inclusion of wheel slip increases the realism of the system but also poses significant challenges in the design and tuning of control parameters.

For backstepping controllers, the coefficients k_1, k_2, k_3 play a crucial role in ensuring that positional and directional deviations converge to zero [23,24]. Under ideal conditions, when the assumption of non-slip rolling is satisfied, these parameters can be chosen relatively flexibly [25]. However, when wheel slippage occurs, the relationship between wheel velocity and the robot's actual motion is distorted, leading to the virtual control signals in the backstepping design no longer accurately reflecting the actual kinematics. This makes the system more sensitive to parameter selection, and inappropriate k_1, k_2, k_3 values can cause prolonged oscillations, reduced trajectory

tracking accuracy, or local instability during complex motion phases.

Simulation results show that, in the presence of wheel slip, increasing the backstepping coefficients to improve convergence speed is not always effective, as it may increase the required velocity amplitude and create conflicts with the lower-stage SMC controller. This shows that the problem of selecting and determining the backstepping parameter under conditions of wheel slip is a multi-objective optimization problem. This ensures a balance between trajectory tracking accuracy, control signal continuity, and system robustness.

6. Conclusions

In this study, we presented the development of a kinematic and dynamic model for a TWMR that considers lateral and longitudinal wheel slip effects. A hierarchical control structure was designed, combining a backstepping controller for the kinematic level and an SMC controller for the dynamic level. The proposed approach enables the robot to track a predefined trajectory under different operating conditions.

To address the slippage issue, a limiting moment was introduced to ensure that the applied torque does not exceed the frictional force generated at the wheel–ground interface. Simulation results demonstrated the effectiveness of the proposed control scheme in maintaining stable and accurate trajectory tracking performance.

In future work, advanced parameter tuning approaches will be investigated to further improve system performance under wheel slip conditions. Metaheuristic optimization algorithms such as Particle Swarm Optimization (PSO), Genetic Algorithm (GA), and Differential Evolution (DE) have shown potential in determining optimal control parameters based on criteria such as tracking error, control effort, and robustness [26]. In addition, artificial intelligence techniques, including neural networks and reinforcement learning, may provide adaptive capabilities for handling uncertainties and varying slip conditions.

Furthermore, Hedge Algebra is considered a promising approach for parameter tuning in nonlinear control systems of mobile robots. Compared to traditional fuzzy logic control (FLC), it provides a more rigorous mathematical framework for modeling linguistic variables while overcoming some limitations in highly nonlinear and uncertain environments [27]. The integration of Hedge Algebra into the tuning of backstepping and SMC parameters could improve adaptability without requiring precise modeling of wheel–ground interaction dynamics.

Author contributions

Long Q. Dinh: Conceptualization, Methodology, Writing – original draft. Dung T. Nguyen: Software, Validation, Data curation. Duc M. Ngo: Formal analysis, Investigation. Mui D. Nguyen: Resources, Visualization. Hung T. Nguyen: Investigation, Validation. Ha T. Nguyen: Methodology, Software. Thang C. Vu: Writing – review & editing, Project administration. Minh T. Nguyen: Supervision, Funding acquisition, Writing – review & editing.

Use of Generative-AI tools declaration

The authors did not use any generative AI or AI-assisted technologies in the preparation of this manuscript.

Acknowledgments

The author would like to thank Thai Nguyen University of Technology (TNUT), Viet Nam.

Conflict of interest

All authors declare that there is no conflict of interest.

References

1. Ito J, Murakami T (2023) Underactuated Control for Two-Wheeled Mobile Robot with an Arm Using Torque Constraint Conditions and Disturbance Observer. In *2023 IEEE 32nd International Symposium on Industrial Electronics (ISIE)*, 1-6. IEEE. https://doi.org/10.1109/ISIE51358.2023.10228153
2. Dinh QL, Nguyen T (2025). Metaheuristic Algorithms to Determine PID Controller Parameters for Mobile Robots. *Journal of Electrical and Electronics Engineering* 18: 27-32.
3. Liu H, Shen Y, Yu S, Gao Z, Wu T (2024) Deep reinforcement learning for mobile robot path planning. *arXiv preprint arXiv:2404.06974*.
4. Klančar G, Škrjanc I (2007) Tracking-error model-based predictive control for mobile robots in real time. *Robot Auton Syst* 55: 460-9. https://doi.org/10.1016/j.robot.2007.01.002
5. Tran HT, Tran DT, Nguyen MT, Vu TC (2024) Intelligent mobile robot for contagious disease treatments in hospitals. *MethodsX* 13: 102941. https://doi.org/10.1016/j.mex.2024.102941
6. Ullah I, Adhikari D, Khan H, Anwar MS, Ahmad S, Bai X (2024) Mobile robot localization: Current challenges and future prospective. *Comput Sci Rev* 53: 100651. https://doi.org/10.1016/j.cosrev.2024.100651
7. Panigrahi PK, Bisoy SK (2022) Localization strategies for autonomous mobile robots: A review. *J King Saud Univ-Com Inform Sci* 34: 6019-39. https://doi.org/10.1016/j.jksuci.2021.02.015
8. Nguyen MD, Vu TC, Hoang VT, Nguyen DT, Nguyen TV, Dinh LQ, et al. (2025) Fusion of Wheel Encoded Data and RFID Signals using Kalman Filter for Robot Indoor Localization. *Journal of Future Artificial Intelligence and Technologies* 2: 328-42. https://doi.org/10.62411/faith.3048-3719-126
9. Tran HT, Tran DL, Nguyen MT (2024) Design of a robotic system to assist in the treatment of severe COVID-19 patients. *Advanced Control for Applications: Engineering and Industrial Systems* 6: e193. https://doi.org/10.1002/adc2.193
10. Siciliano B, Khatib O, Kröger T (Eds.) (2008) *Springer Handbook of Robotics*, Springer-Verlag. https://doi.org/10.1007/978-3-319-32552-1
11. Dinh LQ, Nguyen DC, Hai DT, Vu NP, Long BT, Puta H, et al. (2025) Metaheuristic algorithms for PID controller parameters tuning: approaches and results. In: Nguyen DC, Hai DT, Vu NP, Long BT, Puta H, Sattler KU, editors. *Advances in Engineering Research and Application. ICERA 2024. Lecture Notes in Networks and Systems*, vol. 1611. Cham: Springer. https://doi.org/10.1007/978-3-032-03859-3
12. Tran HT, Tran DL, Pham QN, Vo TC, Nguyen QN, Nguyen TK, et al. (2023) Field programmable gate array based moving object tracking system for robot navigation. *Bulletin of Electrical Engineering and Informatics* 12: 771-81. https://doi.org/10.11591/eei.v12i2.4538
13. Yigit S, Sezgin A (2023) Trajectory tracking via backstepping controller with PID or SMC for mobile robots. *Sakarya University Journal of Science* 27: 120-34. https://doi.org/10.16984/saufenbilder.1148158

14. Yang Y, Yan X, Sirlantzis K, Howells G (2019) Application of sliding mode trajectory tracking control design for two-wheeled mobile robots. In *2019 NASA/ESA Conference on Adaptive Hardware and Systems (AHS)*, 109-114. IEEE. https://doi.org/10.1109/AHS.2019.00012
15. Nghiem GK, Le TL, Phung TC, Dinh QH (2025) A study on the optimal control strategy using sliding mode controller for Mecanum-Wheeled omnidirectional mobile robot. *Measurement* 255: 118113. https://doi.org/10.1016/j.measurement.2025.118113
16. Fierro R, Lewis FL (1997) Control of a nonholomic mobile robot: Backstepping kinematics into dynamics. *Journal of robotic systems* 14: 149-63. https://doi.org/10.1002/(SICI)1097-4563(199703)14:3<149::AID-ROB1>3.0.CO;2-R
17. Hadi NH, Younus KK (2020) Path tracking and backstepping control for a wheeled mobile robot (WMR) in a slipping environment. In *IOP Conference Series: Materials Science and Engineering* 671: 012005). IOP Publishing. https://doi.org/10.1088/1757-899X/671/1/012005
18. Ullah Z, Xu Z, Lei Z, Zhang L (2018) A robust localization, slip estimation, and compensation system for WMR in the indoor environments. *Symmetry* 10: 149. https://doi.org/10.3390/sym10050149
19. Le HN, Pham MK, Pham DH, Nguyen TV (2025) Trajectory tracking and stabilization of two-wheeled balancing mobile robot with hierarchical and sliding mode control. *International Journal of Dynamics and Control* 13: 10. https://doi.org/10.1007/s40435-024-01518-0
20. Camino A, Villegas A, Pérez E, López R, Andaluz GM, Leica P (2024) Cascade Control Based on Sliding Mode for Trajectory Tracking of Mobile Robot Formation. *Engineering Proceedings* 77: 13. https://doi.org/10.3390/engproc2024077013
21. Gao Y, Zhao C, Kang S, Li L, Asano F (2024) Modeling and Simulation of a Wheel-less Omnidirectional Robot Moving in Isotropic Environment. *In 2024 International Symposium on Intelligent Robotics and Systems (ISoIRS)*, 38-42. IEEE. https://doi.org/10.1109/ISoIRS63136.2024.00015
22. Kalin M, Jan P (2025) Understanding the friction laws of Amontons and Coulomb by evaluating the real contact area. *Friction* 13: 9440986. https://doi.org/10.26599/FRICT.2025.9440986
23. Hasanlu M, Siavashi M (2025) Fuzzy adaptive back stepping control of wheeled mobile robot. *Robotic Systems and Applications* 5: 12-27. https://doi.org/10.21595/rsa.2025.24708
24. Li R, Han X, Luo X (2025) Trajectory Tracking Control of Rehabilitation Mobile Robots Based on Fuzzy Backstepping Method. In *2025 5th International Conference on Computer, Control and Robotics (ICCCR)*, 1-5. IEEE. https://doi.org/10.1109/ICCCR65461.2025.11072660
25. Hassani I, Rekik C (2023) Backstepping controller for mobile robot in presence of disturbances and uncertainties. *International Journal of Robotics and Control Systems* 3: 934-54. https://doi.org/10.31763/ijrcs.v3i4.1110
26. Sachan S, Swarnkar P. Investigations on meta-heuristic algorithms for intelligent speed regulation of mobile robot. *Results in Control and Optimization* 11: 100232. https://doi.org/10.1016/j.rico.2023.100232
27. Mac TT, Vu TD, Bui QD, Le MQ, Nguyen ST, Nguyen XT (2025) The development of an optimal hedge algebras path following controller for Robotnik. *Intelligent Service Robotics* 18: 1231-47. https://doi.org/10.1007/s11370-025-00638-6

AIMS Press